ALEPH 99-069
CONF 99-043

Abstract 7-413

Search for invisible Higgs boson decays in e^+e^- collisions at a centre-of-mass energy of 188.6 GeV

The ALEPH Collaboration

PRELIMINARY

Abstract

In a data sample of 176.2 pb^{-1} collected in 1998 by the ALEPH detector at a centre-of-mass energy of 188.6 GeV, invisible decays of a Higgs boson have been searched for in the reaction $e^+e^- \to hZ$, where the Z can decay into e^+e^-, $\mu^+\mu^-$or $q\overline{q}$. No evidence for a signal is found. For a production cross section equal to that of the Minimal Standard Model Higgs boson, masses below 95.4 GeV/c^2 are excluded at 95 % C.L.

(*ALEPH contribution to the 1999 summer conferences*)

Contact: kado@lal.in2p3.fr

1 Introduction

Higgs boson decays into invisible final states are predicted by various extensions of the Standard Model [1]. In these models, the reaction $e^+e^- \to hZ$ leads to topologies involving acoplanar pairs of leptons or jets. The production cross section can be expressed as $\xi^2\sigma_{SM}(e^+e^- \to HZ)$, where ξ^2 is a model-dependent factor which reduces the cross section with respect to that of the production of the Standard Model Higgs boson H.

Invisible Higgs boson decays have already been searched for in the data collected by ALEPH up to 184 GeV [2]. The events selected in the data were found to be compatible with the Standard Model expectations. Similar results have been obtained by DELPHI [3]. The search reported here is based on data collected by ALEPH in 1998 at a centre-of-mass energy of 188.6 GeV, with an integrated luminosity of 176.2 pb^{-1}.

2 The ALEPH detector

The ALEPH detector and its performances have been described in Refs. [4, 5, 6]. The tracking system consists of a silicon vertex detector, a cylindrical drift chamber and a large time projection chamber. A magnetic field of 1.5 T provided by a superconducting coil allows a charged particle $1/p_T$ resolution of $(6 \times 10^{-4} \oplus 5 \times 10^{-3}/p_T)$ GeV/c^{-1} to be achieved.

Electrons and photons are identified by using the information from the electromagnetic calorimeter, providing a measurement of their energy with a relative resolution of $0.18/\sqrt{E} + 0.009$ (E in GeV). The iron return yoke is instrumented and used as a hadronic calorimeter and, together with external chambers, allows muon identification. It provides a measurement of the hadronic energy with a relative resolution of $0.85/\sqrt{E}$ (E in GeV). The coverage is rendered hermetic down to 34 mrad from the beam axis by two sets of luminosity calorimeters.

The information of all the subdetectors is combined in an *energy flow* algorithm which provides a list of *particles* used to determine the total energy with a resolution of $(0.6\sqrt{E} + 0.6)$ GeV and to form jets with a typical angular resolution of 20 mrad both in azimuthal and polar angles.

3 Event selection

The topologies of interest consist of a pair of leptons or a pair of jets with an invariant mass close to m_Z and with large missing energy and missing mass. The signal topologies were simulated at several Higgs boson masses with the HZHA generator [7]. Large Standard Model background Monte Carlo samples were used to optimize the selection procedures. Dilepton processes were simulated with KORALZ [8] for $\mu^+\mu^-$ and $\tau^+\tau^-$ production, and with UNIBAB [9] for Bhabha scattering. The $\gamma\gamma$ interactions were simulated with PHOT02 [10], PYTHIA [11] and PHOJET [12], depending on the specific kinematic configurations and final states. A private generator was used to simulate $Z\nu\bar{\nu}$ final states [13]. All other relevant processes ($q\bar{q}$, WW, ZZ, Weν and Zee) were simulated

with PYTHIA. Additional simulations of the $q\overline{q}$ and WW backgrounds were performed using the KORALZ and KORALW [14] generators.

The selection criteria were optimized by minimization of the expected 95 % C.L. cross section upper limit in the absence of signal, as determined from Monte Carlo simulations (the $\overline{N}_{95}$ prescription [15]). In the optimization procedure, following the prescription advocated in [16], the irreducible background coming from ZZ production was fully subtracted, but only 80 % of the other backgrounds. However, to derive the final results, all backgrounds were fully subtracted, with systematic uncertainties taken into account as prescribed in [17].

In the following, unless otherwise specified, all efficiency and background values, and all numbers in general, pertain to the analysis designed for a 95 GeV/c^2 signal mass hypothesis.

3.1 The acoplanar lepton pair topology

To select hZ final states where the Z decays leptonically and the Higgs boson invisibly, events are required to have only two good tracks, which must be identified either as an electron pair or a muon pair. Only leptons well contained in the detector are selected by requiring $|\cos\theta_{1,2}| < 0.95$, where $\theta_{1,2}$ are the polar angles of the leptons with respect to the beam axis. In addition, the acollinearity, defined as the angle between the two lepton directions, is required to be greater than 125°.

To reject the background from $e^+e^- \to e^+e^-$ and $\mu^+\mu^-$, the visible energy is required to be less than 65 % of the centre-of-mass energy and the acoplanarity, defined as the azimuthal angle between the two lepton directions, must be less than 178°. The background contribution from the $\gamma\gamma \to \ell^+\ell^-$ processes is reduced by requiring the total transverse momentum p_T to be greater than 10 GeV/c.

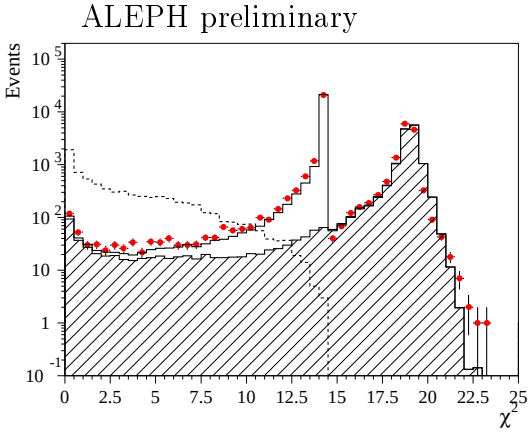

Figure 1: Distribution of the χ^2 for the data (dots with error bars), and the background (full histogram). The contribution from dilepton events is indicated (shaded). The signal distribution is also shown with an arbitrary normalization (dashed histogram)

From the measured transverse momenta of the two leptons and their error estimates, a χ^2 measuring the consistency of the lepton pair mass with the Z mass is minimized. The χ^2 distribution is shown in Fig. 1 for data and Monte Carlo, after the requirement of two identified leptons. Events with a χ^2 greater than 5.0 are rejected.

The signal efficiency is 33 %, corresponding to 0.7 signal events expected, while 4.5 events are expected from the background (2.5 WW, 1.4 ZZ, 0.4 $\tau^+\tau^-$, 0.2 e^+e^- and $\mu^+\mu^-$). Five events were selected in the data.

The systematic uncertainty on the efficiency was estimated to be 6 % (relative), dominated by the limited Monte Carlo statistics, the lepton identification and tracking resolution. The uncertainty on the background estimation is 8 % (relative), dominated by lepton identification and tracking resolution.

3.2 The acoplanar jet pair topology

3.2.1 Event selection

The acoplanar jet pair topology closely resembles that which arises from the $e^+e^- \to H\nu\bar{\nu}$ reaction. The main differences with respect to the search for the standard $H\nu\bar{\nu}$ final state arise from the Z and Higgs boson exchanged rôles: the missing mass is now due to the Higgs boson, and the visible mass to the Z. Furthermore, b-tagging is less powerful than for the standard search, but nevertheless allows some additional efficiency to be gained when the Z decays into $b\overline{b}$.

Therefore, an approach largely inspired from one of those developed in [16] to search for the $H\nu\bar{\nu}$ final state is used here: the two most important backgrounds, $q\overline{q}(\gamma)$ and WW+Weν, are handled by dedicated Neural Networks (NNs). Since the selection is very similar to the "3-fold-NN" analysis described in Ref. [16], only the changes with respect to that analysis are detailed hereafter.

At the preselection level, the missing mass cut is relaxed in order to remain efficient for low invisible Higgs masses: $\not\!\!M > 30$ GeV/c^2. The visible mass must be smaller than 120 GeV/c^2.

The $q\overline{q}(\gamma)$ background rejection is addressed by a 7-variable neural network (7V-NN) similar to the one of [16], but with the missing mass replaced by the visible mass.

After the preselection, ~ 405 events are expected from the WW background, most of them being from semi-leptonic final states involving τ leptons. The anti-WW preselection of [16] is first applied. To reject further those events where a W decays into $\tau\nu_\tau$, one-prong τ candidates are reconstructed. To take into account τ decays involving π^0s, up to four photons within a cone of 10° around the direction of the charged particle track are clustered to it in increasing order of angular distance, as long as the total invariant mass of the cluster is smaller than 1.5 GeV/c^2. Tau candidates are required to have a momentum larger than 3 GeV/c. The isolation of a τ candidate is defined as the energy contained within a 30° cone around its direction, excluding the τ cluster energy. This isolation energy, the distribution of which is shown in Fig. 2, is required to exceed 5 GeV.

As in [16], further rejection of the WW background is achieved using a 3-variable neural network (3V-NN), here again with the missing mass replaced by the visible mass. Since in this analysis, b-tagging cannot be used as in [16] to reject the Weν background, the 3V-NN is trained with an admixture of WW and Weν events.

The final selection criteria consist of requirements placed upon the rarities of the two neural networks, where the rarity of an event is defined as the fraction of signal events which are less signal like with respect to the considered variable. The distributions of the two NN rarities are shown in Fig. 3 for all backgrounds and for the data after all

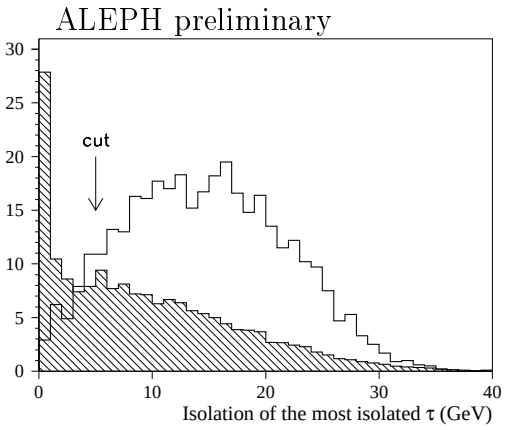

Figure 2: Distributions of the isolation of the most isolated τ for signal (hollow) and WW events (hatched), after the standard anti-WW preselection. The cut is indicated by an arrow.

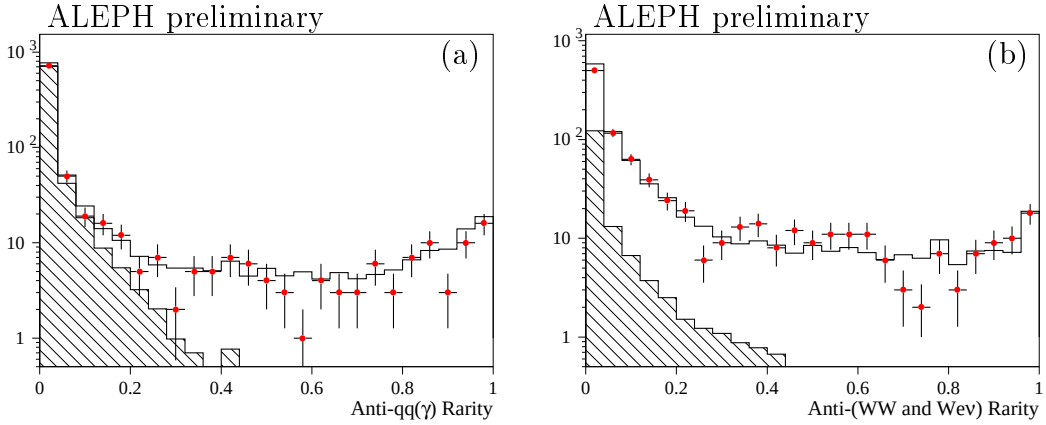

Figure 3: Distributions of the rarity of the anti-q$\overline{\text{q}}(\gamma)$ 7V-NN output (a) and of the rarity of the the anti-(WW+Weν) 3V-NN output (b) for the background (histograms) and the data (points with error bars). Contributions from q$\overline{\text{q}}(\gamma)$ (a) and WW and Weν (b) events are indicated as hatched histograms.

preselection cuts; the signal distributions are uniform by construction. A working point is determined, using the $\overline{N}_{95}$ prescription, by independently varying the cuts on both rarities. The cut values for this "general branch" are 0.30 and 0.29 for the 7V-NN and 3V-NN rarities, respectively.

As was already done in [2], one can further benefit from the fact that ~ 22 % of the hadronic Z decays are into b$\overline{\text{b}}$ to apply looser cuts for well b-tagged events. Here, events are considered as well b-tagged if $\eta_1 + \eta_2$ is greater than 1.5, where $\eta_{1,2}$ are the b-tag NN outputs for the two best tagged jets in the event. The cut values of 0.45 and 0.10 in this "b-tag branch" are determined in order to obtain the best performance for the "OR" of the two branches. The improvement achieved by adding the b-tag branch is indeed marginal at high Higgs boson mass; however, it is significant for masses around 80 GeV/c^2 where the WW and Weν backgrounds dominate.

Finally, as in [16], a cut on E_{12}, the amount of energy detected within 12° of the

beam axis, is applied. This cut principally addresses radiative $q\overline{q}$ events where a photon is detected at low angle. The cut value of 1 % $\sqrt{s}$ was optimized taking into account the beam related background, based on the information from events triggered at random beam crossings. The inefficiency due to this cut is typically of the order of 1 %.

At the working point, the signal efficiency is 38.6 % (taking into account the systematic corrections discussed further down). This efficiency corresponds to 7.8 signal events expected to be detected, while 12.4 events are expected from standard background processes (8.0 ZZ, 0.9 WW, 1.5 Weν, 1.8 $q\overline{q}$ and 0.2 Z$\nu\bar{\nu}$). In the data, 14 events were selected.

In order to achieve a reasonably uniform performance on a large invisible Higgs mass interval, neural networks were trained for various signal mass values (70, 75, 80, 85, 88, 90, 92 and 95 GeV/c^2), and the cuts on the rarities were optimized for each of those masses. This procedure effectively copes with the change of background composition when going from Higgs boson masses around 80 GeV/c^2, where the WW and Weν backgrounds dominate, to $\sim$ 90 GeV/c^2 where the ZZ background dominates. For mass values intermediate between those for which NNs were trained, interpolated cuts are applied on the interpolated rarities.

Altogether, a total of 44 events are observed, while 47.6 events are expected from Standard Model processes (taking into account the corrections discussed below). As shown in Fig. 4, a maximum of 23 events are selected for any given Higgs boson mass hypothesis.

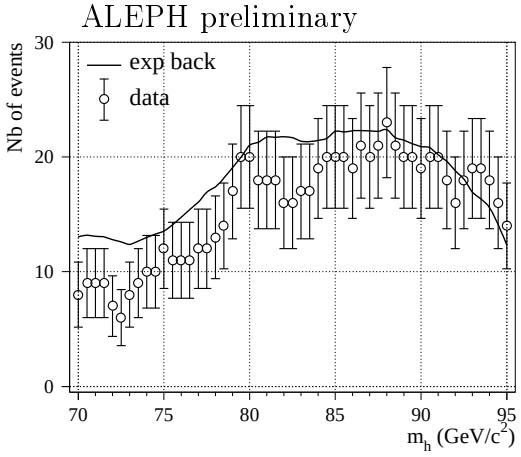

Figure 4: Expected number of events (solid line) and number of candidate events (points with error bars) as a function of the Higgs boson mass.

3.2.2 Systematic studies

Systematic effects related to the energy resolution and calibration and to the jet direction reconstruction have been studied using hadronic events collected at the Z peak in 1998. Except for the fact that no flavour selection is performed, the procedure is identical to the one described in [16]. As a result, the efficiencies for the signal — and for the irreducible ZZ and Z$\nu\bar{\nu}$ backgrounds — are reduced by 1 % to 2 % (relative), depending on the mass hypothesis. The simulation of the anti-WW preselection variables has also been

studied with the Z peak data sample, resulting in efficiency reductions smaller than 0.2 % (relative). Half of these corrections are taken as systematic uncertainties.

The Weν cross section computed with PYTHIA is 20% larger than the value obtained with GRACE4f [18]. Since the latter generator is expected to produce a more accurate result for this cross section, the amount of Weν background is corrected accordingly, and half of this correction is taken as systematic uncertainty.

The remaining $q\overline{q}$ background, initially estimated with PYTHIA, is dominated by double radiative events. A study using the KORALZ generator, which is expected to simulate the initial state radiation more accurately, indicates that PYTHIA underestimates this background (by almost a factor three for the 95 GeV/c^2 mass hypothesis). A correction is therefore applied accordingly to the $q\overline{q}$ background estimate, and half of this correction is taken as systematic uncertainty.

To further check the WW and thus modified Weν Monte Carlo predictions in the signal region, a sample of data events enriched in WW and Weν events is selected. For this purpose, the nominal cut on the 7V-NN output is applied to reject most of the $q\overline{q}$ events remaining after the preselections. About 87 events are expected from the standard processes, among which 42 and 24 originate from WW and Weν, respectively, while 77 events are selected in the data. Subtracting from both the observed and expected numbers of events the contribution from the other (mostly ZZ) backgrounds, the observed deficit in the data leads to a correction factor of 0.8 ± 0.1, where the error is dominated by the size of the data sample. Given the limited statistics, this correction is assumed to be constant over the whole range of 3V-NN outputs.

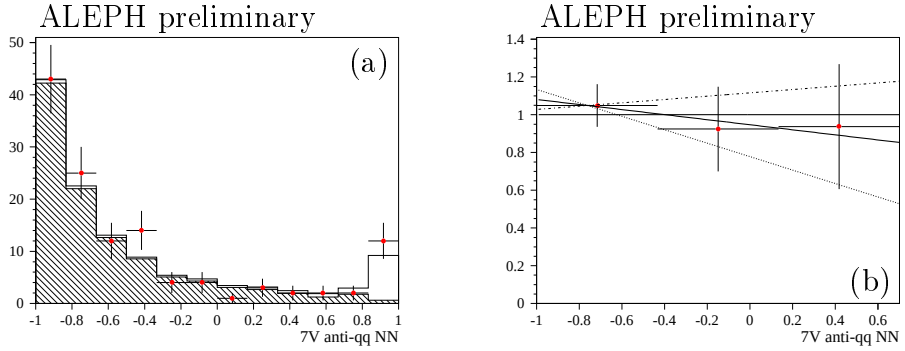

Figure 5: Distribution of the anti-$q\overline{q}(\gamma)$ 7V-NN for the background (histogram, with the $q\overline{q}(\gamma)$ contribution shown hatched) and the data (points with error bars) (a) and their ratio (b). The linear fit to this ratio is also shown, together with the lines corresponding to one standard deviation from this fit.

A similar procedure is used for the $q\overline{q}$ background. A data sample enriched in double radiative events (which constitute the bulk of the ultimate $q\overline{q}$ background) is selected by applying the nominal cut on the 3V-NN output, after all preselections. A total of 124 events are observed in the data, while 121 are expected from the simulation, among which 105 double radiative events. The distribution of the 7V-NN output for these events is shown in Fig. 5(a). The $q\overline{q}$ background level in the signal region is determined from a linear fit to the data/Monte Carlo ratio for values of the 7V-NN output smaller than

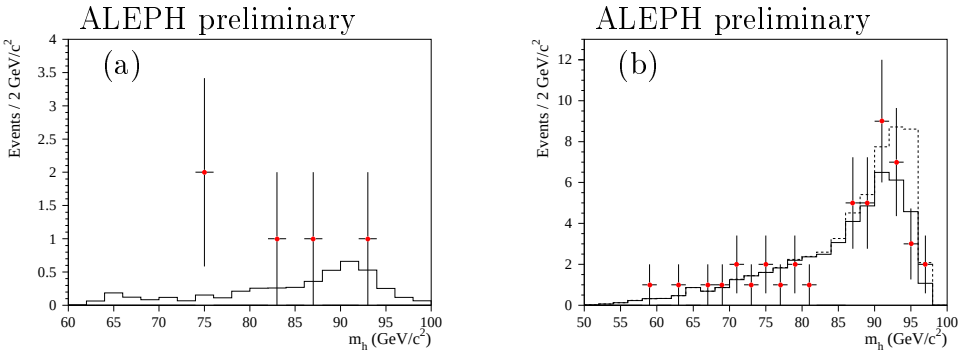

Figure 6: Distribution of the reconstructed Higgs boson mass in the leptonic (a) and hadronic (b) channels for the data (points with error bars) and for the background (full histograms). The contribution of a 95 GeV/c^2 mass Higgs boson signal is also shown for the hadronic channel (dashed histogram).

0.7 (corresponding to the nominal rarity cut), as shown in Fig. 5(b). Extrapolating the result of the fit into the signal region (*i.e.*, to 7V-NN output values larger than 0.7), the correction factor is determined to be 0.83 ± 0.35, where the error is dominated by the data statistics.

4 Combined results

Overall, a total of 49 events are selected, combining the leptonic and hadronic channels, in agreement with the 52.1 events expected from all Standard Model background processes. The distributions of the Higgs boson mass, reconstructed with the Z mass constraint applied to the visible system, are shown in Fig. 6 for both the leptonic and hadronic channels.

The combined observed and expected confidence levels are shown in Figure 7(a). The confidence levels for background only are shown in Figure 7(b). These confidence levels have been calculated with the same statistical procedure as in Ref. [16].

The result of this analysis can alternatively be presented as an exclusion domain in the (m_{h}, ξ^2) plane, as shown in Fig. 8. For Higgs bosons produced with the Standard Model cross section and decaying invisibly, the expected 95% CL limit is 94.4 GeV/c^2. The mass lower limit obtained is 95.4 GeV/c^2.

5 Conclusions

Searches for invisible decay modes of the Higgs boson produced in the reaction $\mathrm{e^+e^-} \to \mathrm{hZ}$ have been carried out in the acoplanar jet and acoplanar lepton topologies using 176.2 pb^{-1} of data collected by ALEPH at a centre-of-mass energy of 188.6 GeV. No excess with respect to the Standard Model has been found in the data, yielding a lower limit of 95.4 GeV/c^2 for the mass of an invisibly decaying Higgs boson produced with a cross section equal to that of the Standard Model Higgs boson.

References

[1] For a review, see: M. Carena and P.M. Zerwas (Conveners) *et al.* in "Higgs physics at LEP2", Ed: G. Altarelli, T. Sjöstrand, and F. Zwirner, CERN-96-01 (1996) 351.

[2] The ALEPH Collaboration, *Phys. Lett.* **B450** (1999) 301.

[3] The DELPHI Collaboration, CERN-EP/99-059, to be published in *Phys. Lett. B.*

[4] The ALEPH Collaboration, *Nucl. Instrum. Methods* **A294** (1990) 121.

[5] D. Creanza *et al.*, *Nucl. Instrum. Methods* **A409** (1998) 157.

[6] The ALEPH Collaboration, *Nucl. Instrum. Methods* **A360** (1995) 481

[7] P. Janot, "The HZHA generator", in Physics at LEP 2, Eds. G. Altarelli, T. Sjöstrand and F. Zwirner, CERN 96-01 (1996) 309.

[8] S. Jadach and Z. Was, *Comput. Phys. Commun.* **36** (1985) 191.

[9] H. Anlauf *et al.*, *Comput. Phys. Commun.* **79** (1994) 466.

[10] J.A.M. Vermaseren in Proceedings of the IVth International Workshop on Gamma Gamma Interactions, Eds. G. Cochard, P. Kessler, Springer Verlag, 1980;
The ALEPH Collaboration, *Phys. Lett.* **B313** (1993) 509.

[11] T. Sjöstrand, "The PYTHIA 5.7 and JETSET 7.4 Manual", LU-TP 95/20; CERN-TH 7112/93 (1993, revised August 1994); *Comput. Phys. Commun.* **82** (1994) 74.

[12] R. Engel, *Z. Phys.* **C66** (1995) 203;
R. Engel and J. Ranft, *Phys. Rev.* **D54** (1996) 4144.

[13] This generator is based on the differential cross section published in
S. Ambrosanio and B. Mele, *Nucl. Phys.* **B374** (1992) 3.

[14] M. Skrzypek, S. Jadach, W. Placzek, and Z. Was, *Comput. Phys. Commun.* **94** (1996) 216.

[15] J.-F. Grivaz and F. Le Diberder, *"Complementary analyses and acceptance optimization in new particle searches"*, LAL-92-37.

[16] The ALEPH Collaboration, "Search for the neutral Higgs Bosons of the Standard Model and the MSSM in e^+e^- collisions at $\sqrt{s} = 188.6$ GeV", ALEPH 99-053, CONF 99-029, submitted to the HEP99 Conference, Tampere, Finland, Abstract 7-428.

[17] R. D. Cousins and W. L. Highland, *Nucl. Instrum. Methods* **A320** (1992) 331.

[18] J. Fujimoto *et al.*, *Comput. Phys. Commun.* **100** (1997) 128.

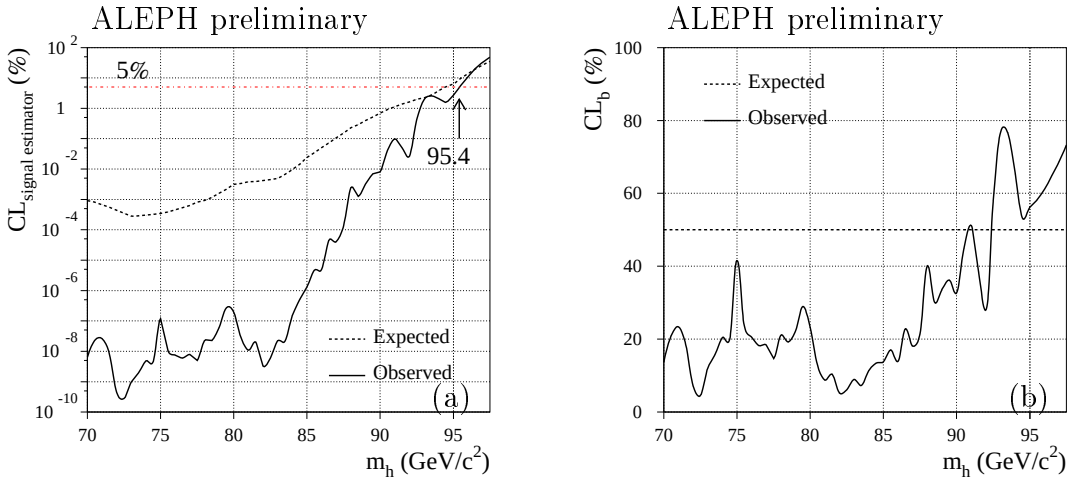

Figure 7: Signal estimator confidence levels (a) for the combination of the leptonic and hadronic channels. The confidence levels for background only are also displayed in (b).

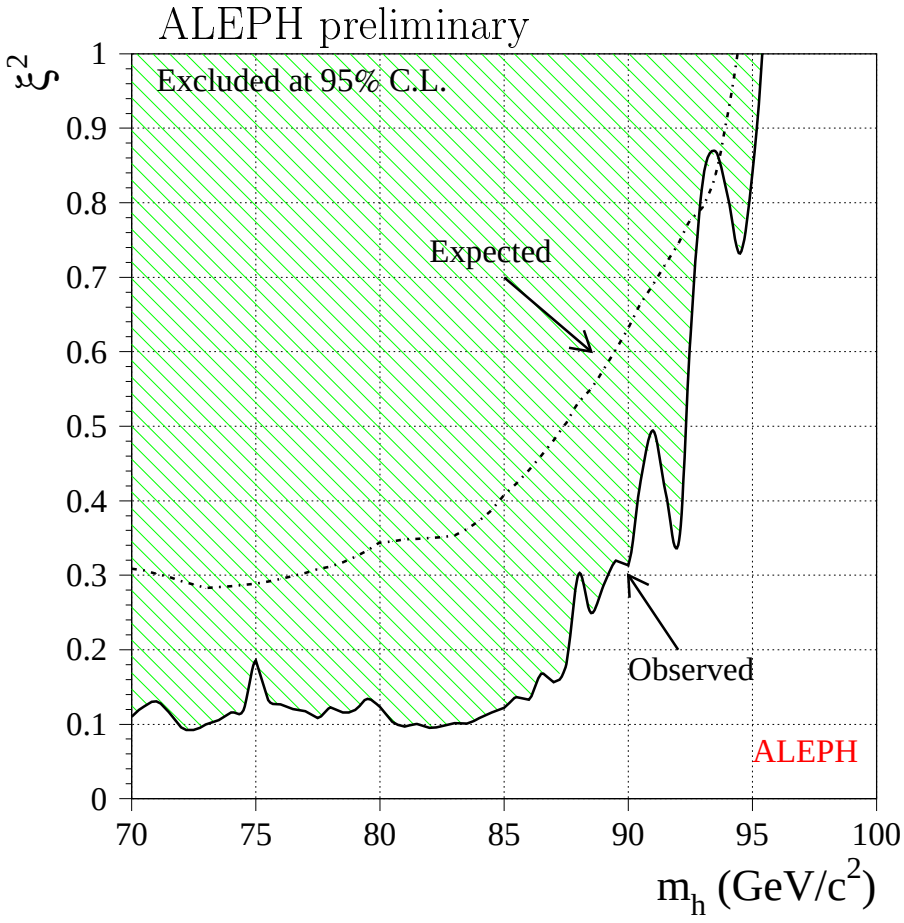

Figure 8: Excluded region at the 95 % C.L. in the $(m_{\rm h}, \xi^2)$ plane.